2014

Magnetic Battery Feasibility Study using Flux Switching Topology

Andrew W. Janzen

John R. Natzke
George Fox University, jnatzke@georgefox.edu

Magnetic Battery Feasibility Study using Flux Switching Topology

Andrew W. Janzen, John R. Natzke, Ph.D.

Electrical Engineering Department, George Fox University, Newberg, OR 97132 USA

Permanent magnets have long been known to store magnetic energy in the alignment of the magnetic domains within the material. This paper investigates the possibility of constructing a magnetic device which can effectively extract the stored potential energy from permanent magnets and convert that energy into electrical energy. The concept stemmed from a number of patents which claimed to effectively extract energy from strong neodymium or samarium cobalt magnets on a macroscopic scale using specially designed magnetic flux paths. Their method uses one of several different techniques to switch permanent magnet flux between alternating paths and electrical energy is extracted from coils intercepting this flux as it changes within the core. Using experimental testing, magnetic simulations, and theoretical predictions, our research examined this question. The experimental results indicate that the devices tested do not effectively extract magnetic energy from the magnetized materials under test, indicating that the design is not suitable for use as a magnetic battery.

***Index Terms*—magnetic battery, magnetic energy, magnetic conversion efficiency, permanent magnets.**

I. Introduction

There are several factors which make magnetic battery concepts appealing technologies. Magnets can be magnetized very quickly, which enables rapid magnetic recharging. This type of battery, if operational, could be used in high power electric vehicles and other high power electronics. Because of the powerful coercive forces of conventional Nd-Fe-B magnets, the magnets can maintain their magnetic state for many years without demagnetizing, providing an inherent advantage over conventional batteries which lose charge over time. For a magnetic battery of the flux switching topology to function, the energy provided to the switching coils by the input circuitry must be less than the amount of energy extracted at the output.

Originally, it was thought that this could be justified due to the large amount of energy which is used to magnetize the magnets and due to demagnetization over time when magnets are loaded magnetically. The flux switching topology has been known for over 40 years and has been the focus of several patents which aim to use the topology to extract energy from the magnets generating the flux [4], [10].

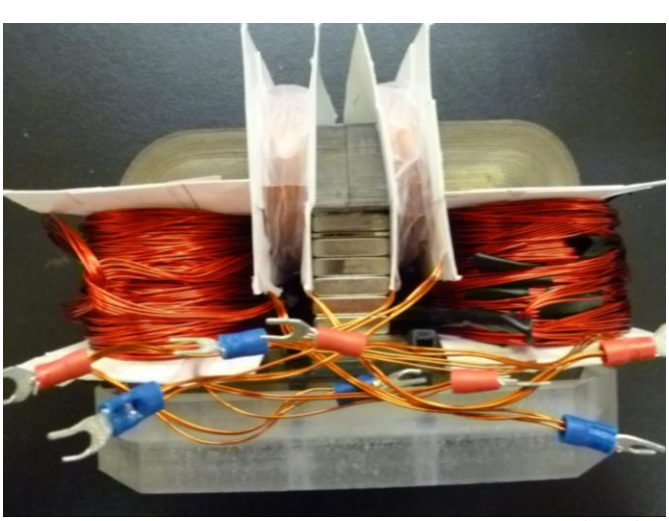

Fig. 1. Magnetic battery prototype 1 uses control coils to perform flux switching. The prototype was based on United States patent 6362718.

Conceptually, a magnetic battery uses static flux from at least one permanent magnet to provide the necessary flux for the battery's operation. This static flux is usually switched using control coils to provide an increase or decrease in the flux along at least two alternate flux paths. The patents assumed that the amount of energy required to switch the static field of the magnet was less than the amount of energy which could be extracted from the magnet during the flux switching process.

This assumption, however, was not confirmed in this research. The research provided no evidence that the addition of magnets increased the output power from the device, although in certain configurations the magnets did perform as flux switches.

Fig. 2. Magnetic battery prototype 2 uses cross flux switching to couple switching flux to the output coil. The prototype was based on United States patent 7830065. Outer sheet-steel casing (flux return path) not shown.

Although the magnet does increase the stored energy in the core, the output coil is incapable of extracting this energy since an output voltage is only induced when there is a change in the magnetic flux; thus a static flux does nothing to contribute to output power in this configuration. Due to this, both experimental prototypes performed as expected with efficiencies under 100%.

In order to switch flux from a permanent magnet, the permeability of at least one of the flux paths must be varied to provide an increase or decrease in flux on that path. There are many ways of doing this. The most common method uses control coils to increase or decrease the permeability of a region of the core. Other approaches use rotating superconductors or capacitive flux switches to alternately switch flux between the paths. Using control coils is the simplest method as the flux is directly modulated in each of the paths and this approach is similar to conventional transformer operation.

The second prototype used a very unique cross flux switching design where the control flux is always applied perpendicular to the magnets and the output coil is perpendicular to the input coil. Thus, all the coupling from input to output is performed indirectly using flux switching within the core.

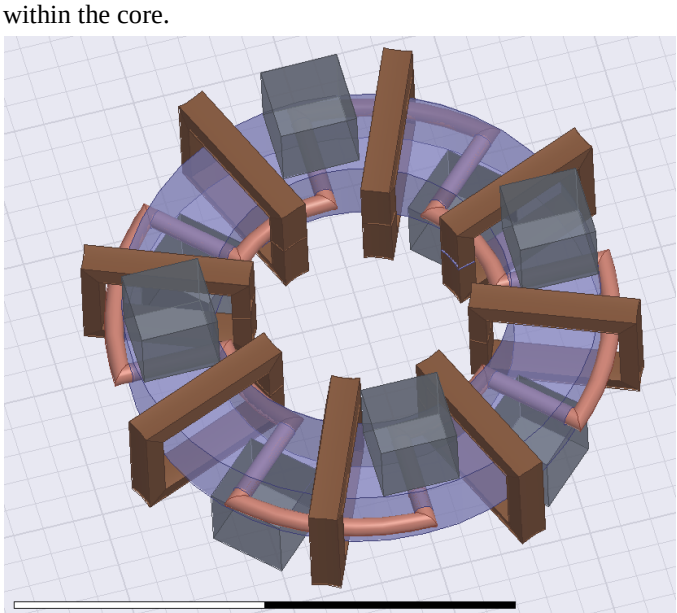

Fig. 3. Simulated geometry of magnetic battery prototype 2 demonstrating the complex winding pattern design.

II. Theoretical Background

1) Theoretical magnetostatic model of prototype 1 and 2

Using equations (1) to (5), the flux through a core can be approximated assuming uniform flux distribution, isotropic core permeability, and no flux leakage as described in [5]:

$$MMF = Hl = NI \quad (1)$$

$$B = \mu H = \frac{\mu NI}{l} \quad (2)$$

$$R = \frac{l}{\mu A} \quad (3)$$

$$MMF = \phi R \quad (4)$$

$$\phi = BA = \frac{\mu NIA}{l} \quad (5)$$

The equations are written in terms of magnetomotive force (MMF), path reluctance (R), path flux (ϕ), magnetic flux density (B), material magnetic permeability (μ), coil electric current (I), and the number of turns (N).

Prototype 1 had a core cross-sectional area (A_c) of 1750 mm^2, a magnet cross-sectional area (A_m) of 968 mm^2, a section height ($l_{af} = l_{cd}$) of 65 mm, a section length ($l_{ab} = l_{fe} = l_{bc} = l_{ed}$) of 55 mm, a magnet height ($l_m = l_{gap}$) of 40 mm, a core depth (d) of 70 mm, and a core relative permeability (μ_r) of 398,000 in the linear region [9]. The two

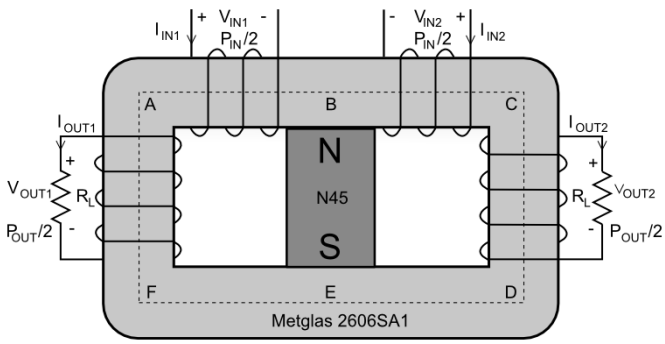

Fig. 4. Simplified geometry used in calculating the theoretical static magnetic flux of prototype 1.

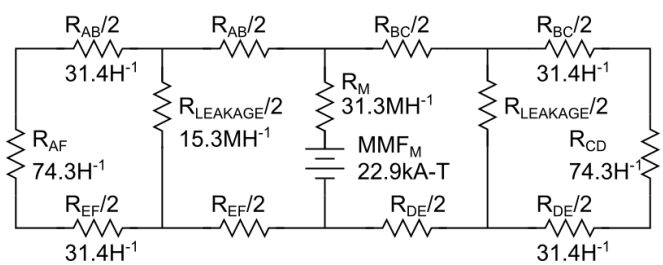

Fig. 5. Circuit representation of the static magnetic circuit in prototype 1.

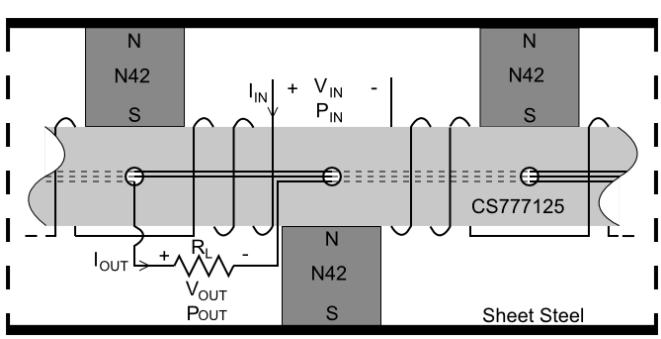

Fig. 6. Partial view of prototype 2 showing three of the eight magnets and the terminations of both the input and output coils. The outer casing is a flux return path made of sheet steel.

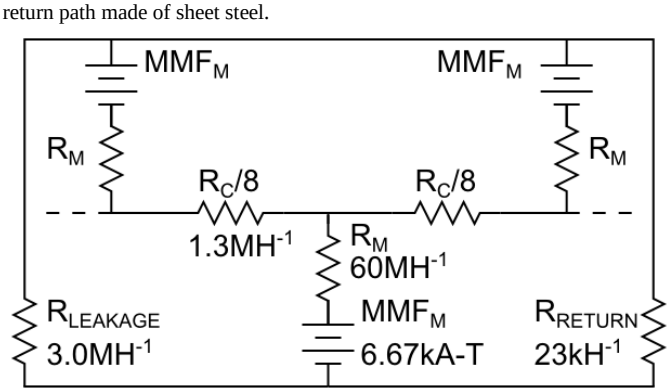

Fig. 7. Partial circuit representation of the static magnetic circuit in prototype 2 showing three of the eight magnets.

input coils each had 40 turns and a mean resistance of 4.39 mΩ per turn; the two output coils were each 45 turns and 1.50 mΩ per turn.

Prototype 2 had an outer diameter of 77.8 mm, an inner diameter of 49.2 mm, and a height of 12.7 mm. The core cross-sectional area (A_c) was 182 mm^2, the mean path length (l_m) was 200 mm, and the core relative permeability (μ_r) was 125 [2]. Each magnet was a 12.7 mm cube. The input coil had 100 turns and a mean resistance of 916 μΩ per turn; the output coil was 48 turns and 190 mΩ per turn.

Using the B-H curves from the Appendix, the net magnet coercive force was iteratively calculated to be 7.2 kOe for prototype 1 and 6.6 kOe for prototype 2 [1],[2],[6],[7],[9]. Due to partial saturation of the core in prototype 2, a relative core permeability value of 87.5 was used for calculations. Using the theoretical model, the static flux through each path was calculated to be 366 μWb or 0.378 T for prototype 1 and 55.5 μWb or 0.314 T for prototype 2.

2) Theoretical magnetodynamic model of prototype 1

When a magnetic field is applied to one of the control coils the flux through each path changes. Since the magnet was assumed to maintain magnetization during flux switching and the core was assumed to have a constant permeability, the static magnetic field from the permanent magnet will have no effect on the theoretical alternating flux through the core. Thus, the prototype can be represented as a magnetostatic model superimposed on a transformer model of the core [5]. The induced voltage (V_{out}) on the output coils can be calculated directly from the transformer model using (6).

$$V = -N\frac{d\Phi}{dt} \tag{6}$$

The equation is a statement of Faraday's law of electromagnetic induction, and defines the relation between the induced voltage (*V*), the number of turns (*N*), and the magnetic flux cutting each loop (Φ). Since a voltage is only induced on an output coil in response to a changing magnetic field, a static permanent magnet will not contribute to a voltage in the output wire. Thus, the magnetostatic model can be ignored when calculating output voltage, leaving only the magnetodynamic transformer model. An ideal transformer can be modeled using the following equations:

$$\frac{V_1}{V_2} = \frac{N_1}{N_2} \tag{7}$$

$$N_1 \cdot I_1 = N_2 \cdot I_2 \tag{8}$$

$$V_1 \cdot I_1 = V_2 \cdot I_2 \tag{9}$$

where N_1 is the number of primary turns, N_2 is the number of secondary turns, V_1 is the primary voltage, V_2 is the secondary voltage, I_1 is the primary current, and I_2 is the secondary current. The equations imply that all the primary energy is coupled to the secondary, thus, an ideal transformer will have an efficiency of 100%. In practice, a magnetic device will have an actual efficiency less than 100% due to core loss and copper loss. Prototype 2 requires a more complex mathematical approach due to the number of magnets and the tensor permeability interactions within the core. Thus, a theoretical model for the device will not be presented here.

3) Device power and efficiency calculations

Device power can be measured at the input and output coils of each prototype as labeled in Figs. 4 and 6. However, the losses in the driver circuit must also be accounted for to properly assess the operation of each device as a magnetic battery. Therefore, the DC drive power supplying the H-bridge circuit was measured, as well as the microcontroller logic power. In this manner, the *drive* efficiency results reported below are based on the input power to the H-bridge, whereas the *total* efficiency results include both the H-bridge and logic power. The two efficiency calculations can thus be defined as

$$\eta_{drive} = \frac{P_{out}}{P_{drive}} \tag{10}$$

$$\eta_{total} = \frac{P_{out}}{P_{drive} + P_{logic}} \tag{11}$$

where

$$P_{drive} = V_{H-bridge} \cdot I_{H-bridge} \tag{12}$$

$$P_{logic} = V_{logic} \cdot I_{logic} \tag{13}$$

$$P_{out} = \frac{V_{out}^2}{R_L} \tag{14}$$

4) Simulation verification

Field pattern simulations for prototypes 1 and 2 were performed using both ANSYS Maxwell and FEMM and are shown in Figs. 8 to 11. Using ANSYS Maxwell 3D and

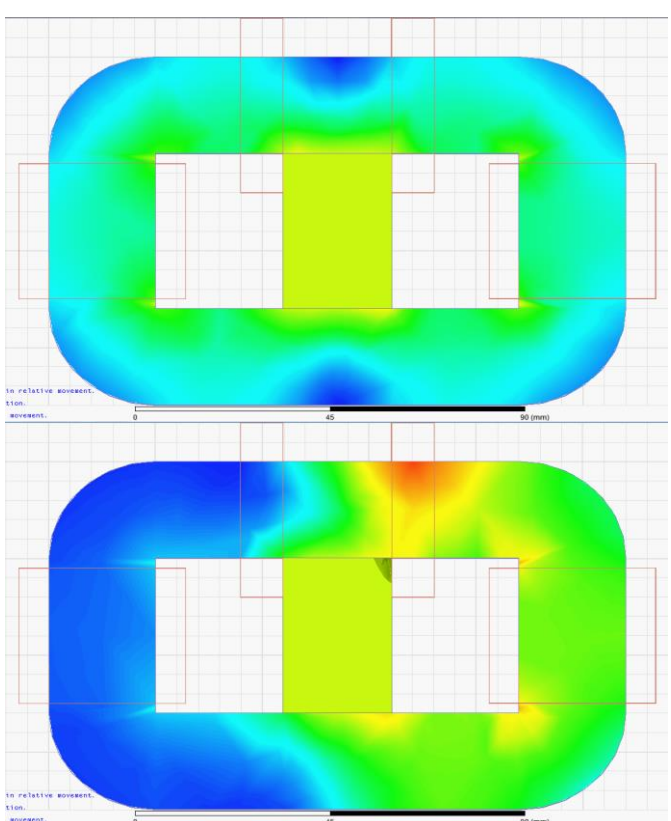

Fig. 8. ANSYS Maxwell simulation of magnetic flux densities in the core of prototype 1 during switching. The field pattern in the upper image shows the field pattern with no switching, and the field pattern shown in the lower image shows the field pattern with full switching current applied.

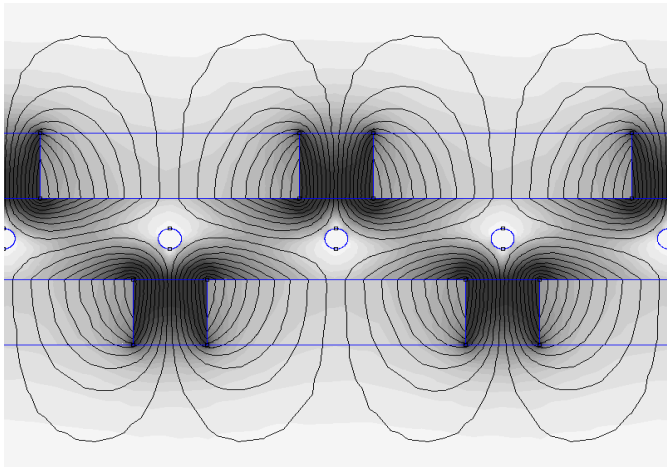

Fig. 9. FEMM simulated field pattern for prototype 2 in air. The field pattern indicates significant flux leakage near the magnets. The model stretches the 3D device into 2D for simulation and thus can only be relied on as a rough approximation.

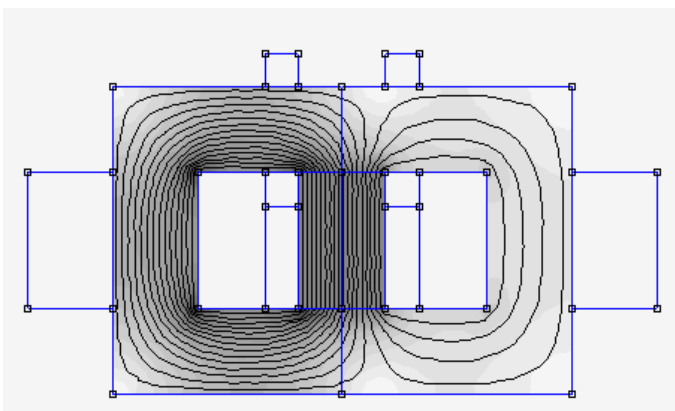

Fig. 10. FEMM simulated field pattern for prototype 1. This simulation includes flux contributions from the input coil, magnet, and the loaded output coils. Simulations indicate that loading the output coils increases the flux density at the inner edges of the core.

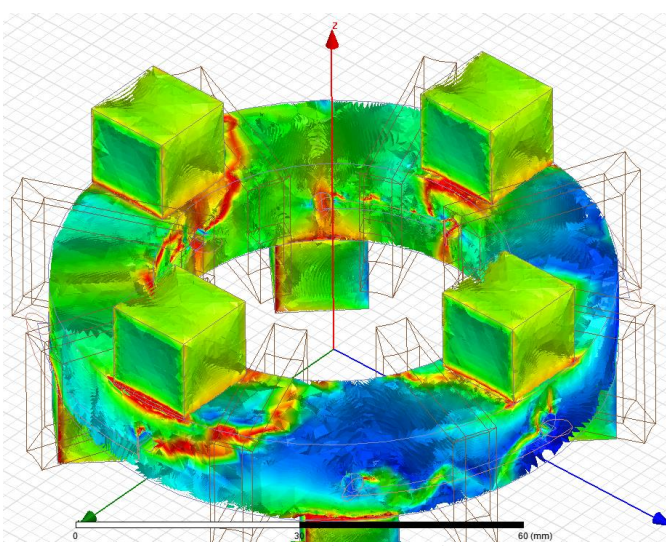

Fig. 11. ANSYS Maxwell simulated field pattern for prototype 2 in air. The field pattern indicates significant flux leakage near the magnets.

accounting for core conductivity and coil resistance, a device efficiency of 96.4% was predicted for prototype 1.

III. Prototype Design

1) *Materials and construction*

Due to the high flux density of the Nd-Fe-B magnets, the core materials required careful selection to prevent core saturation. For prototype 1, the Metglas 2605SA1 core was chosen to provide high saturation flux density, low eddy current loss due to the use of thin laminations, high frequency response, and low hysteresis loss. To achieve the unique shape required by prototype 2, a machinable, low loss, powdered iron composite CS77125 was chosen. Prototype 1 used a stack of seven N45 magnets, and prototype 2 used eight N42 magnets. See the Appendix for material B-H curves.

2) *Circuit configuration and design*

A custom high efficiency driver circuit was designed to source 5 A at 80 V to the control coils at frequencies up to 450 kHz; see Fig. 12. The microcontroller and H-bridge driver were the circuit's most significant sources of loss.

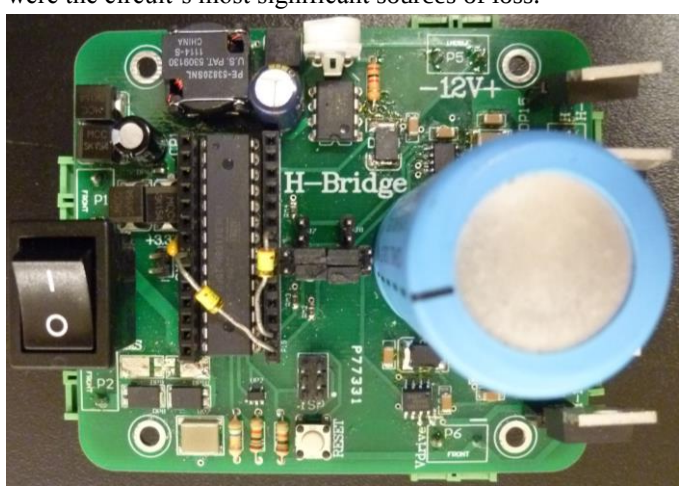

Fig. 12. Driver circuit used to perform input coil switching.

IV. Device Testing

Both prototypes were tested over the full operating range of the driver circuitry, over a wide range of load values from open circuit to short circuit, and over a range of operating voltages. Interestingly, both devices produced waveforms which were very similar, in spite of the differences in geometry. Results are shown in Figs. 13 to 18.

1) *Measured power and efficiency data for prototype 1*

Total efficiency is influenced by core, copper, and circuit losses. Optimization was achieved by sweeping a range of operating frequencies, load resistances, and drive voltages. The maximum total efficiency was 83.0% and the maximum drive efficiency was 94.0%. These efficiencies were achieved at an operating frequency of 10.0 kHz, a drive voltage of 17.6 V, and a load resistance of 617 Ω. This experimental result is less than the simulated efficiency of 96.4%, most likely due to using a simulation model which ignored core hysteresis. During these measurements no decrease in output voltage or power was observed with time, suggesting that no energy was being extracted from the magnet. Removing the magnet from prototype 1 and conducting the same testing procedures resulted in only a 1.0% change (increase) in device efficiency.

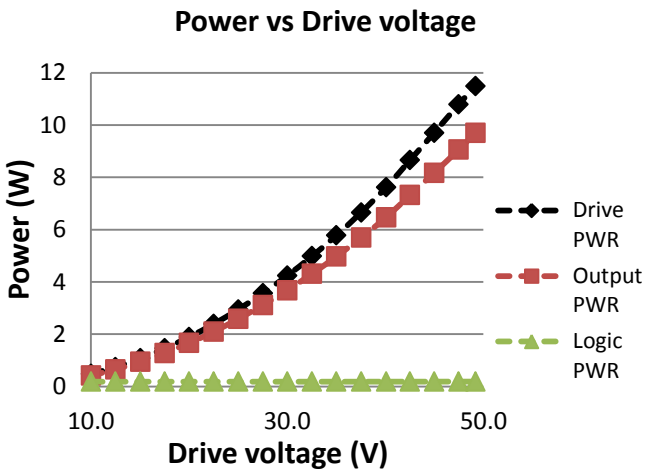

Fig. 13. Power vs. voltage curves for drive, input, and logic power for prototype 1. The data indicate a constant power to the drive circuitry but an increasing input and output power with increasing voltage. The logic power is a higher percentage of the net power at low drive voltages. This results in a lower efficiency at low drive voltages.

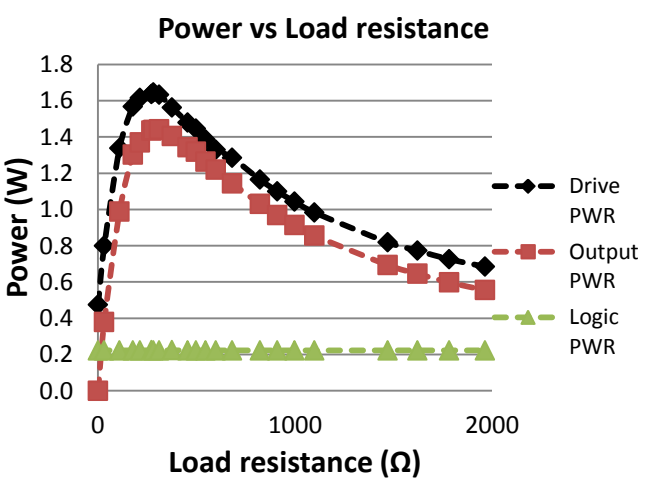

Fig. 14. Power vs. load resistance curves for drive, input, and logic power for prototype 1. The turns ratio, the coil resistance and the coil inductance at the operating frequency all help determine the optimal load resistance value.

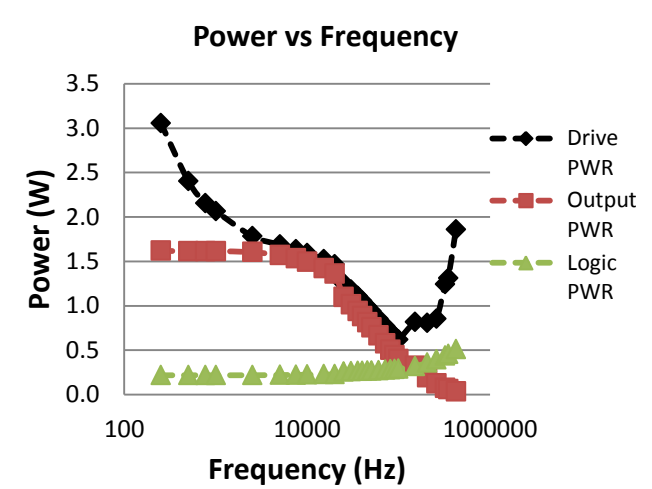

Fig. 15. Power vs. frequency curves for drive, input, and logic power for prototype 1. The logic power required increases with frequency and the output power decreases with frequency.

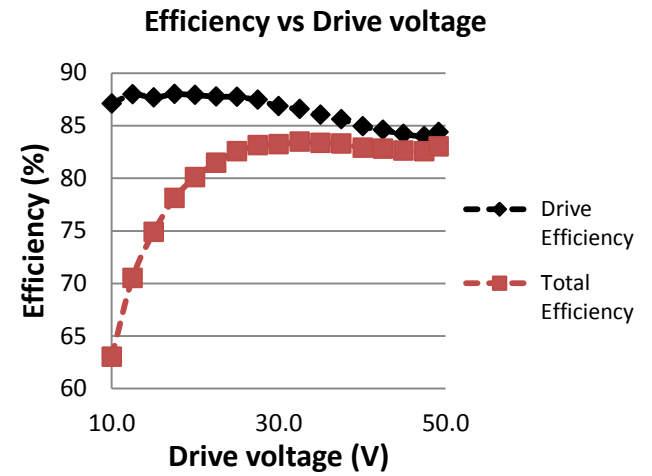

Fig. 16. Total efficiency and drive efficiency over drive voltage for prototype 1. Drive efficiency excludes the contribution of logic input power from the efficiency calculation.

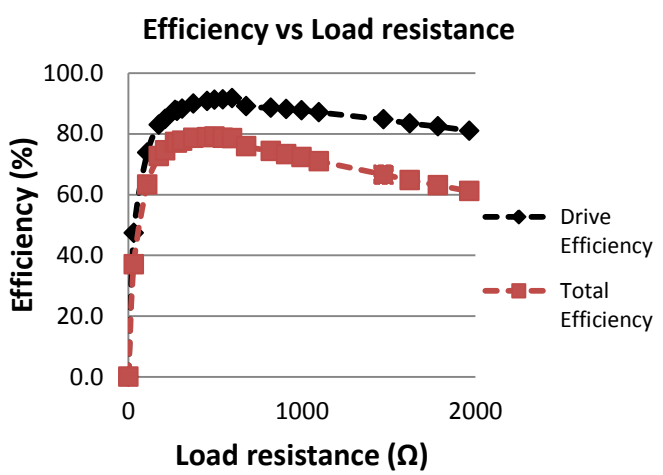

Fig. 17. Total efficiency and drive efficiency at different load resistance values for prototype 1 at the optimal drive voltage of 17.6 V.

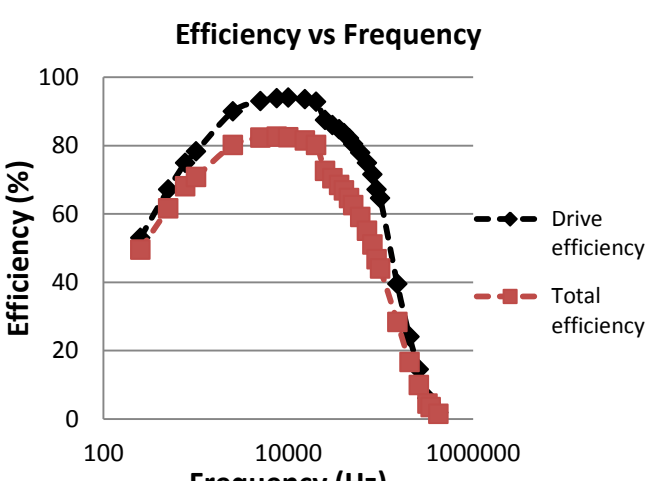

Fig. 18. Total efficiency and drive efficiency over frequency for prototype 1 at an optimal drive voltage of 17.6 V and load resistance of 617 Ω.

2) Measurements for prototype 2

The results for the second prototype were surprisingly similar, differing only slightly in the average output voltages, efficiency, and maximum power. The second prototype had a maximum total efficiency of 78.5% and a maximum drive efficiency of 88.5%. These efficiencies were both less than those for prototype 1 due to the increased core loss in the powdered iron core used in prototype 2. As with prototype 1, no decrease in output voltage or power was observed over time.

When the magnets were removed from prototype 2, no output voltage was detected, even though the same field was applied as when the magnets were in place. Because the input and output coils are perpendicular to each other, the coils will not couple, and thus an alternating magnetic field at the input will not generate a corresponding voltage in the output. The presence of permanent magnets alters the field pattern creating a permeability tensor in the core. This allows the changing input magnetic field to modulate the flux from the magnets and thereby modify the field in a perpendicular direction, generating a voltage in the output coil. This operation would not be seen for prototype 1 since the coils are directly coupled.

3) Field strength measurements for prototypes 1 and 2

Field strength measurements were conducted on the permanent magnets after testing and compared to identical reference magnets from the same lot. For both prototypes, the reference magnets and the magnets used in testing gave identical average readings to within the precision of the Tesla meter. The magnets used in prototype 1 gave an average reading of 0.541 T, and the magnets for prototype 2 gave 0.525 T. These results, along with the repeatable power measurements during device testing, indicate that no significant amount of demagnetization occurred for the magnets of either prototype.

According to convention, another indicator of the lack of demagnetization would be that the ratio of the input coil MMF to the permanent magnet MMF was always much less than unity. For example, during experimentation with prototype 1, the maximum MMF of either input coil was 11.6 A-t; given the magnet MMF from Fig. 5, the resulting MMF ratio was 5.08×10^{-4}. Therefore, demagnetization could not have occurred in a direct manner. However, even if the MMF ratio was to surpass unity for these devices, the flux switching topologies were intentionally designed to minimize if not avoid any direct demagnetization of the magnets.

V. Conclusions

As the experimental data show, the devices consistently operated with efficiencies less than 100%, supporting the previously mentioned theoretical predictions and simulation results. Even though the magnets bias the core in a higher magnetic state, they do not provide a means to extract that energy in a macroscopic way. With the ratio of the input coil MMF to the permanent magnet MMF much less than unity, demagnetization could not occur, and thus energy could not be extracted, unless by some other mechanism. But the flux switching topologies under test provided no such mechanism. Although it is always possible to overlook the key to an invention, present results indicate that the claimed patent operation is not possible. From the testing accomplished by the authors, it has been shown that these devices are not feasible for use as magnetic batteries.

Despite these results, unexpected insights into possibly new magnetic concepts have proven quite encouraging. The operation of the prototypes was different from the operation of a conventional transformer in significant ways. In both prototypes the cores were magnetically biased, and flux from the magnets was switched back and forth within the core. For prototype 1, the magnet's presence did not cause a significant change to the device's power efficiency for the given materials, though this effect could be investigated further. In the case of prototype 2, the presence of the magnets created a tensor permeability which allowed flux from the input coil to couple to the perpendicular output coil.

The second prototype was specifically designed to load the magnets rather than the input circuitry to improve the conversion efficiency, and although the conversion efficiency remained below 100%, the prototype only operated when the magnets were in place. In other words, the second prototype operated as a flux switch. This type of device could be used as a power proximity sensor, which provides output power only when the magnets are very close to the core. The configuration could also be used as a motor, where the magnet flux is to be switched back and forth using the cross flux technique demonstrated in prototype 2 rather than using more conventional flux switching methods. With further research, other applications might be demonstrated for such a device as this.

APPENDIX

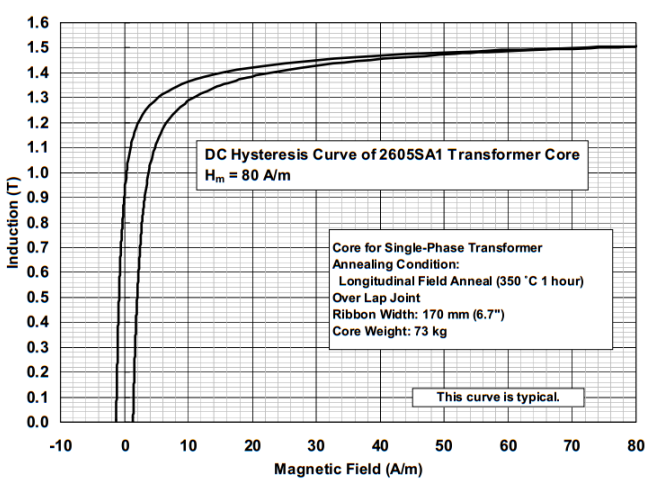

Fig. 19. B-H curve for Metglass Inc. 2605SA1 transformer core used in prototype 1.

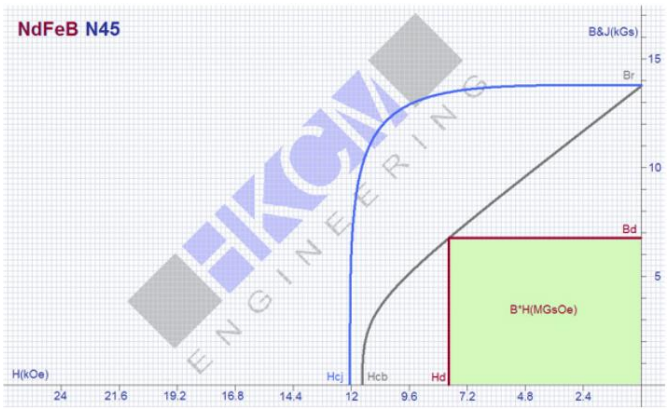

Fig. 20. B-H curve for HKCM Engineering Neodymium N45 magnet used in prototype 1.

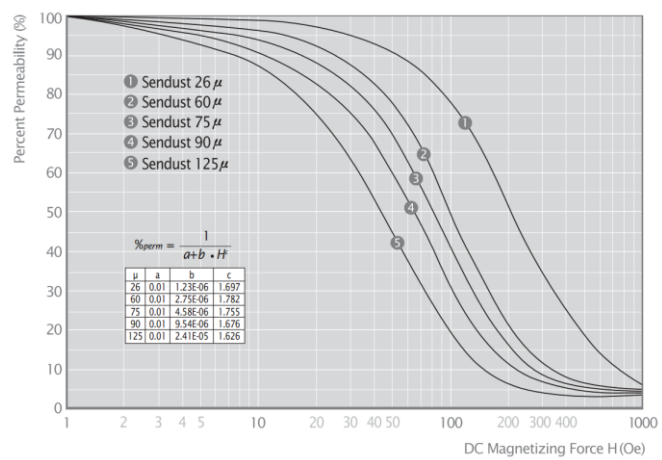

Fig. 21. Percent permeability vs DC magnetizing force curves for various Sendust composites. For prototype 2 the core material used was Sendust 125µ.

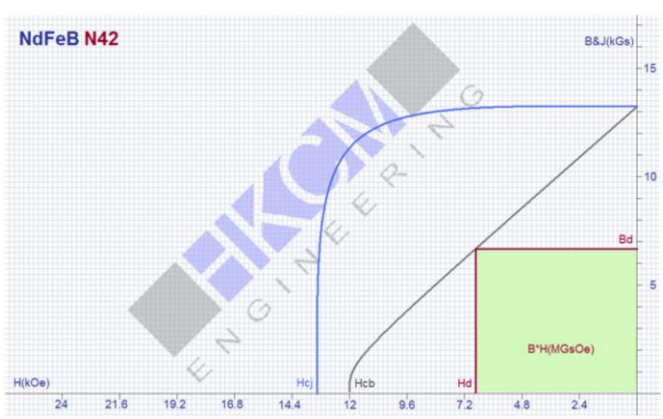

Fig. 22. B-H curve for HKCM Engineering Neodymium N42 magnet used in prototype 2.

ACKNOWLEDGEMENTS

This work was supported in part by an undergraduate Richter Scholars research grant through George Fox University. The authors would like to thank Joseph Stupak and Dr. Ed Godshalk for their contributions and suggestions during the research.

REFERENCES

[1] Changsung Corporation. "Magnetic Powder Cores - Technical Data." *Percent Permeability vs DC Bias Curves - Sendust Alloy Powder.*

[2] Changsung Corporation. "Toroidal Magnetic Powder Cores." *OD777 - Sendust CS777125.*

[3] G. Gogue and J. Stupak, *Theory and Practice of Electromagnetic Design of DC Motors and Actuators*. Oersted Technology, 1993.

[4] G. Gunderson, "Solid state electric generator," U.S. Patent 7 830 065. Nov. 9, 2010.

[5] B. Guru and H. Huseyin, *Electric Machinery and Transformers*. 3rd ed. New York, NY: Oxford University Press, 2001.

[6] HKCM Engineering. "Neodymium (NdFeB) N42," *BH-diagram demagnetization curve*. June 2014.

[7] HKCM Engineering. "Neodymium (NdFeB) N45," *BH-diagram demagnetization curve*. July 2013.

[8] J. C. Maxwell. *A Treatise on Electricity and Magnetism*, 3rd ed., vol. 2. Oxford: Clarendon, 1892.

[9] Metglas, Inc. *Amorphous Alloys for Transformer Cores.* Metglas 2605SA1. Technical datasheet, 2011.

[10] P. Stephen et al. "Motionless electromagnetic generator," U.S. Patent 6 362 718. Mar. 26, 2002.

[11] W. H. Yeadon, *Handbook of Small Electric Motors.* New York, NY: McGraw-Hill, 2001.

[12] F. Ulaby, *Fundamentals of Applied Electromagnetics*, 6th ed. Upper Saddle River, NJ: Pearson Prentice Hall, 2010.